Physical Equivalent Circuit Model for Planar Schottky Varactor Diode

PASCAL PHILIPPE, WALID EL-KAMALI, AND VLAD PAUKER

Abstract—**A physical equivalent circuit model for the planar GaAs Schottky varactor diode is presented. The model takes into account the distributed resistance and capacitance of the active layer, the side-wall capacitance, and the parasitic resistances and accurately accounts for the high series resistance observed near the pinch-off voltage. The dependence of the maximum series resistance on varactor size, frequency, and doping profile has been theoretically investigated and the results agree well with experimental data. The proposed model can be easily used for optimization of planar Schottky varactor diodes with regard to broad-band monolithic VCO constraints.**

I. Introduction

THE ONLY TYPE of varactor compatible with the standard GaAs MMIC process is the planar Schottky varactor diode (PSVD) fabricated on a semi-insulating substrate [1]. The high capacitance ratio needed for wide-band VCO's requires that the PSVD's be biased up to pinch-off voltage, at which the depletion layer reaches the substrate [2]. However, near pinch-off, the effective series resistance to the capacitance reaches a maximum which can be high enough to cause a dip in the output power characteristic of the VCO's or can even cause the oscillation to cease [3]. Therefore a physical electrical model is required which accurately accounts for the series resistance–voltage characteristic of the PSVD's up to pinch-off. The model described herein takes into account the distributed resistance and capacitance of the active layer, the parasitic resistances, and the side-wall capacitance. The side-wall capacitance, which was not fully taken into account in the earlier model of Scott *et al.* [3], is in fact of great importance in the behavior of PSVD's near pinch-off. This is outlined in the results reported below, where interest has been focused on the calculation of the maximum series resistance as a function of the varactor size and the frequency. The influence of the doping profile has also been investigated.

Experimental results are then reported which agree well with theory. Improvement and design of PSVD's are finally discussed with regard to broad-band VCO constraints; these are high capacitance ratio, low minimum capacitance, and low maximum series resistance at pinch-off [4].

Manuscript received April 17, 1987; revised September 11, 1987.

The authors are with the Laboratoires d'Electronique et de Physiqué Appliquée, 3, avenue Descartes, 94451 Limeil-Brevannes, France.

IEEE Log Number 8717983.

II. PSVD Model

A PSVD consists of a Schottky anode and two adjacent ohmic contacts deposited on an N-doped GaAs layer. Its electrical behavior can be modeled by the equivalent circuit shown in Fig. 1(a). The active layer under the anode of length L and width W has to be regarded as a distributed $R-C$ network, with C the capacitance of the depletion layer and R the resistance of the conducting channel. The capacitance C varies with the reverse voltage applied to the anode according to

$$C(V) = \frac{dQ(V)}{dV} \tag{1}$$

where Q is the charge of the depletion layer. Assuming the electron mobility μ to be constant, the channel resistance R varies according to

$$R(V) = \frac{L^2}{\mu\left(Q(V_p) - Q(V)\right)} \tag{2}$$

where V_p is the pinch-off voltage. The Schottky barrier reverse conductance can be neglected at microwave frequencies since it is much lower than the susceptance of the depletion layer. Then, C_s is the side-wall capacitance and R_s the series resistance to the ohmic contacts. Finally, the Schottky anode is assumed to be equipotential and is represented by an effective lumped resistance R_a, which is related to the metallization resistance R_m of one anode finger by

$$R_a = \frac{R_m}{3n} \tag{3}$$

where n is the number of anode fingers. This simplification is usually valid up to 20 GHz for PSVD's with anode fingers up to 200 μm in width.

Taking into account the symmetry, the equivalent circuit in Fig. 1(a) can be reduced to a second-order $R-C$ network in series with R_a as shown in Fig. 1(b), where R_t and C_t are, respectively, the input resistance and the capacitance of the distributed $R-C$ network. They are

$$R_t = \frac{R}{4\theta}\,\frac{\sinh(\theta) - \sin(\theta)}{\cosh(\theta) - \cos(\theta)} \tag{4}$$

$$\frac{1}{\omega C_t} = \frac{R}{4\theta}\,\frac{\sinh(\theta) + \sin(\theta)}{\cosh(\theta) - \cos(\theta)} \tag{5}$$

0018-9480/88/0200-0250$01.00

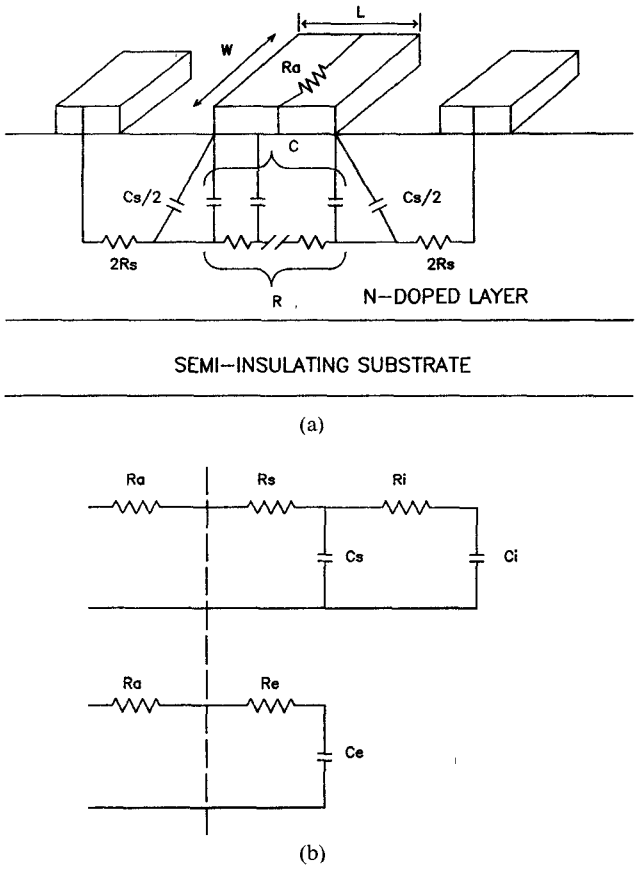

Fig. 1. Equivalent circuit of a planar Schottky varactor diode. (a) Detailed equivalent circuit. (b) Equivalent series $R-C$ network.

where

$$\theta = \sqrt{\frac{RC\omega}{2}}. \tag{6}$$

The second-order $R-C$ network in series with R_a can be transformed into an equivalent first-order network with series resistance and capacitance given by

$$R_e = R_s + \frac{\tau_i C_i}{\omega^2 \tau_i^2 C_s^2 + (C_i + C_s)^2} \tag{7}$$

$$C_e = C_s + \frac{(C_i + C_s) C_i}{\omega^2 \tau_i^2 C_s + (C_i + C_s)} \tag{8}$$

where

$$\tau_i = R_i C_i. \tag{9}$$

The above expressions describe the PSVD behavior up to pinch-off. Fig. 2 shows an example of the theoretical $R_e(V)$ and $C_e(V)$ characteristics calculated at 3 GHz and 10 GHz for a 4 μm$\times$300 μm PSVD with the doping profile (a) depicted in Fig. 3. R_s and C_s are assumed to be voltage independent.

The results may be interpreted as follows:

1) At low voltage ($V \ll V_p$), the distributed effects are negligible ($\theta \ll 1$). Consequently, from expressions (4) and (5), we find $R_i \simeq R/12$ and $C_i \simeq C$, and as $C \gg C_s$, we obtain

$$R_e \simeq R_s + R/12$$
$$C_e \simeq C_s + C.$$

Thus the capacitance C_e of the PSVD is nearly the sum of the depletion-layer and side-wall capacitances while the series resistance R_e is low.

2) At high voltage ($V \gg V_p$), the depletion layer extends into the semi-insulating substrate. Therefore its capacitance C is almost zero. Consequently, R_e and C_e reduce to, respectively,

$$R_e \simeq R_s$$
$$C_e \simeq C_s.$$

3) Just before pinch-off ($V \leqslant V_p$), there is a rapid drop in depletion-layer capacitance and a sharp increase in channel resistance. The series resistance R_e first follows the increase of R_i but it can be demonstrated that a maximum in R_e occurs in the voltage range just before pinch-off, where

$$C_i \leqslant C_s \sqrt{1 + \omega^2 \tau_i^2}. \tag{10}$$

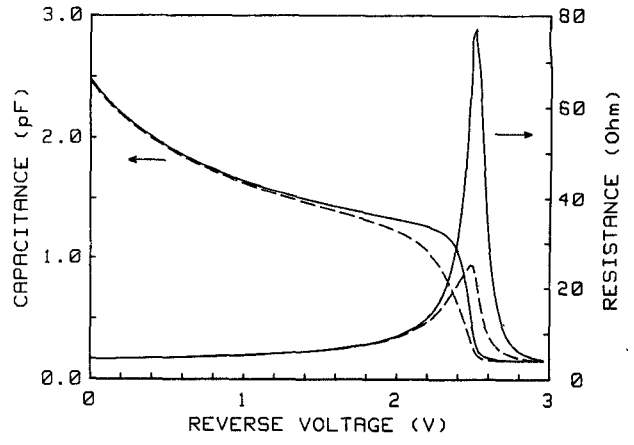

Fig. 2. Theoretical R_e (V) and C_e (V) characteristics of a 4 μm$\times$300 μm PSVD, calculated with the doping profile (a) shown in Fig. 3, and with $R_s = 1\Omega \cdot$mm, $C_s = 0.5$ pF/mm, $\mu = 3000$ cm^2/V/s. Frequency $f = 3$ GHz (solid curves) and $f = 10$ GHz (dashed curves).

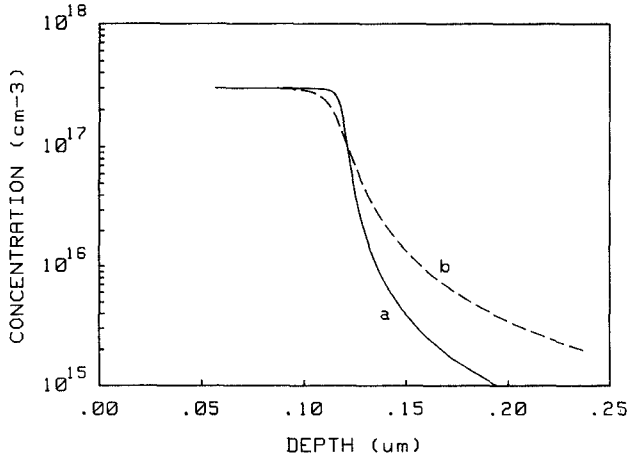

Fig. 3. Doping profiles assumed in theoretical calculations.

If we assume that the increase of R_i and decrease of C_i balance one another so that $\tau_i = R_i C_i$ is almost independent on voltage near pinch-off, a first-order approximation to the maximum series resistance $R_{e,\max}$ can be calculated. It is given by

$$R_{e,\max} \simeq R_s + \sqrt{\frac{K-1}{K+1}} \cdot \frac{1}{2\omega C_s} \tag{11}$$

where

$$K = \sqrt{1+\omega^2 \tau_i^2}\,. \tag{12}$$

The expression (11) shows that $R_{e,\max}$ is inversely proportional to the side-wall capacitance value C_s and decreases with frequency. Moreover, $R_{e,\max}$ increases with the value of τ_i near pinch-off and, hence, with anode length.

The dependence of $R_{e,\max}$ on anode length is illustrated by Fig. 4, which shows the $R_{e,\max}(L)$ characteristics calculated at 3 GHz and 10 GHz with the doping profiles (a) and (b) of Fig. 3. As expected, $R_{e,\max}$ increases with anode length but saturates to an upper limit at a few microns depending on the doping profile and the frequency. The saturation can be explained as follows: since the distributed $R-C$ network is a lossy transmission line, the input wave attenuates while propagating and no change in input impedance will result from an increase in anode length once L is larger than twice the distance at which the propagating wave vanishes (the ratio is 2 because the distributed $R-C$ network is excited at both extremities). Mathematically, the saturation occurs once $\theta > 1$. From (4) and (5), it results that $\tau_i = 1/\omega$, and hence $K = \sqrt{2}$. Placing this value of K into (11), we find the upper limit of the maximum reslstances:

$$R_{e,\max}^{\mathrm{UL}} = R_s + \frac{1}{2\omega C_s(\sqrt{2}+1)}. \tag{13}$$

The expression (13) shows that $R_{e,\max}^{\mathrm{UL}}$ is inversely proportional to the frequency and the side-wall capacitance. The corresponding quality factor Q is independent of frequency. If we neglect the contribution of R_s, it is given by

$$Q = \sqrt{2}+1. \tag{14}$$

Then, since the saturation occurs when $\theta > 1$ at the maximum value of the series resistance, we can estimate the frequency dependence of the saturation length L_s at which the maximum series resistance reaches its upper limit. As

$$\theta = \sqrt{\frac{RC\omega}{2}} \quad \text{and} \quad RC \sim L^2$$

L_s decreases with frequency according to

$$L_s \sim \frac{1}{\sqrt{f}}. \tag{15}$$

The value of the saturation length L_s and the magnitude of $R_{e,\max}$ below the saturation length depend on the doping profile. This is qualitatively illustrated by Fig. 4, which compares the $R_{e,\max}$ versus L characteristics corresponding to the profiles (a) and (b) of Fig. 3. The profiles (a) and (b) have the same doping level and total charge but differ in their doping tail, which extends deeper into the substrate for the profile (b).

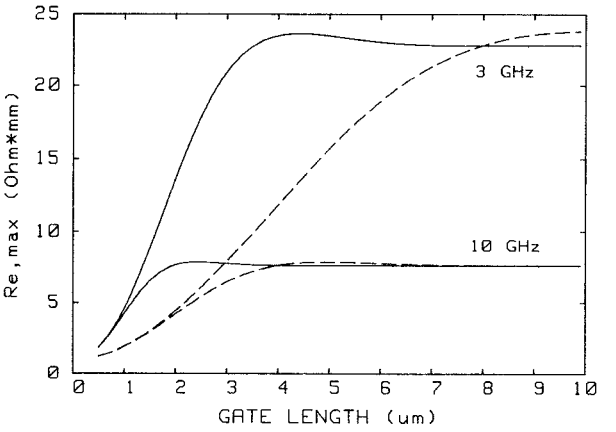

Fig. 4. Theoretical maximum series resistance $R_{e,\max}$ as a function of anode length. Solid and dashed curves have been respectively calculated with the doping profiles (a) and (b) shown in Fig. 3.

Near pinch-off and for a given value of the depletion layer capacitance, the channel resistance is lower for profile (b). Consequently, the input time constant of the distributed $R-C$ network is lower and therefore the saturation length is larger for this profile and the maximum series resistance is lower below the saturation length. This result shows that one can obtain a significant reduction of $R_{e,\max}$ by decreasing the doping gradient of the doping tail which extends into the semi-insulating substrate.

III. Comparison to Experiment

All the PSVD's investigated have been fabricated by ion implantation into GaAs semi-insulating substrate and have four Ti–Pt–Au anode fingers. Their technological and electrical characteristics are listed in Table I, where $C_{\max}$ is the capacitance at zero bias voltage.

Fig. 5 shows the measured $R_e(V)$ and $C_e(V)$ characteristics of PSVD/2a around the pinch-off voltage. These characteristics have been fitted within 5 percent with our model. The circuit element values R, C, and C_s used to provide the best fit have been extracted from measurements by optimization techniques. The resulting variations of R, C, and C_s with bias voltage are shown in Fig. 6. The channel resistance R increases nearly exponentially with voltage while the depletion layer capacitance C decreases abruptly to zero. Using these values of R, C, and C_s, we have calculated the variation of the maximum series resistance $R_{e,\max}$ versus anode length and frequency as, illustrated by Fig. 7. The validity of this computation can be verified by comparing the measured and calculated values of $R_{e,\max}$ for PSVD/1a, which differs from PSVD/2a only in size. The anode length of PSVD/1a is larger than the saturation length above 3 GHz; therefore its maximum series resistance decreases as $1/f$.

TABLE I
PSVD'S INVESTIGATED

PSVD	W (um)	L (um)	Cmax (pF)	Cmin (pF)	Vt (V)
1A	300	5.1	2.55	0.15	3.0
2A	400	3.0	1.95	0.20	3.0
1B	300	5.1	2.25	0.15	8.5
2B	400	3.0	1.80	0.20	8.5

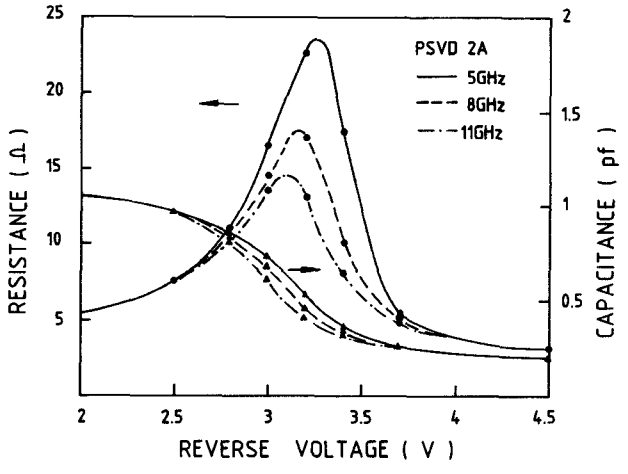

Fig. 5. R_e (V) and C_e (V) characteristics of PSVD/2a around pinch-off.

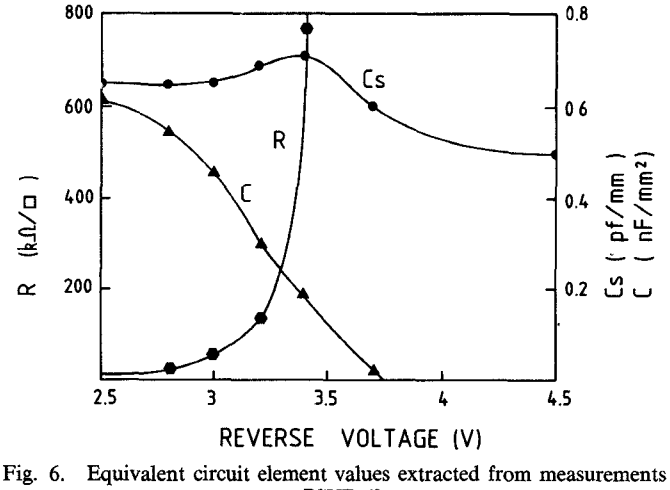

Fig. 6. Equivalent circuit element values extracted from measurements on PSVD/2a.

The influence of the doping profile has been experimentally investigated. Second versions of PSVD/1a and PSVD/2a have been fabricated with a new doping profile, as shown in Fig. 8. For PSVD/1b and PSVD/2b, a second implant has been made deep into the substrate in order to decrease the doping gradient between active layer and substrate. The values of R, C, and C_s have been extracted as before from measurements on PSVD/2b, and Fig. 9 shows the calculated variations of $R_{e,\max}$ with anode length and frequency for the new doping profile. These results are to be compared with those obtained with one implant,

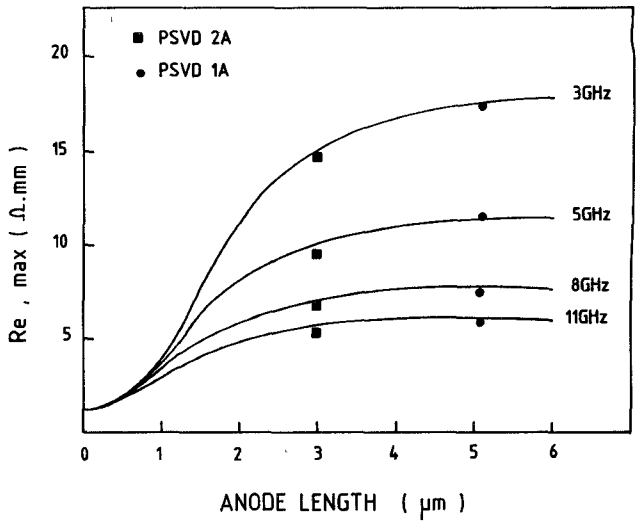

Fig. 7. Maximum series resistance as a function of anode length for single-implantation profile.

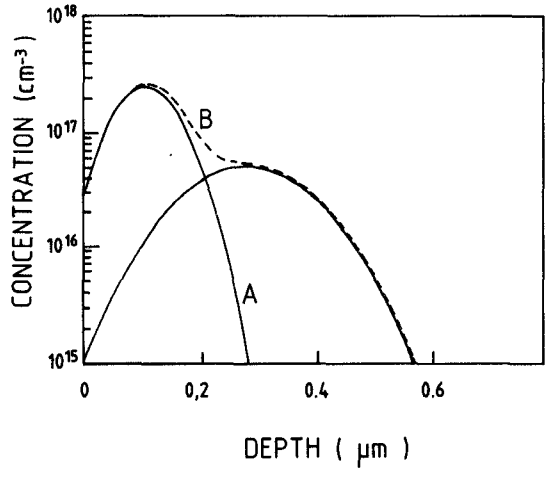

Fig. 8. (a) Single-implantation profile of PSVD/1a and PSVD/2a and (b) double-implantation profile of PSVD/1b and PSVD/2b.

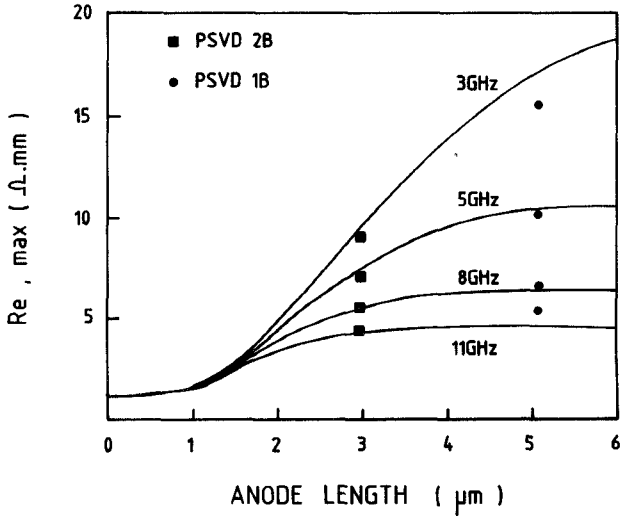

Fig. 9. Maximum series resistance as a function of anode length for double-implantation profile.

shown in Fig. 7. With the double implant, the saturation length has been increased and consequently $R_{e,\max}$ decreased by about 30 percent at 3 GHz for PSVD/2b. For PSVD/1b, the reduction of $R_{e,\max}$ is less significant since its anode length remains close to the saturation length.

IV. Design Considerations

The experimental results are in good agreement with theory for the variation of $R_{e,\max}$ with anode length, frequency, and doping gradient at the substrate interface. This leads us to some considerations for the design of PSVD's with regard to broad-band VCO constraints.

Broad-band monolithic VCO's require a high capacitance ratio $C_{\max}/C_{\min}$, a low minimum capacitance $C_{\min}$, and a low maximum series resistance $R_{\max}$. $C_{\min}$ is equal to the side-wall capacitance value C_s; therefore it depends only on anode width:

$$C_{\min} = C_s \sim W.$$

$C_{\max}$ is composed of the depletion layer capacitance at $V = 0$ (proportional to anode area) and of the side-wall capacitance. Therefore the capacitance ratio $C_{\max}/C_{\min}$ varies with the anode length according to

$$C_{\max}/C_{\min} - 1 \sim L.$$

The size dependence of the maximum series resistance is more complicated. If we neglect the contribution of the anode resistance, $R_{\max}$ may be expressed as

$$R_{\max} = \frac{g(L,f)}{W}$$

where g is a function which increases with anode length and decreases with frequency.

The above relations show that two compromises have to be found when choosing the size of a PSVD. First, a low $R_{\max}$ requires a large anode width, while a small anode width is needed to achieve low $C_{\min}$. Secondly, the small anode length required to obtain low $R_{\max}$ is not always compatible with the length required to achieve the desired capacitance ratio, which is typically a few microns long. Consequently the choice of the geometry of a PSVD is based on a compromise, and if no satisfactory solution can be found, an improvement in the PSVD is necessary. Finally, after the size of the diode has been chosen, the number of anode fingers has to be selected for the anode resistance to have a negligible value. Typically, this requirement is achieved by having anode fingers about 100 μm in width.

V. Large-Signal CAD Model

A large-signal CAD model of PSVD reproducing the behavior described above has been developed for time-domain analysis. The distributed resistance and capacitance of the active layer are simulated by three $R-C$ cells, which have been optimized to fit the input impedance of the distributed $R-C$ network over the largest frequency band. The resistance R and capacitance C of the active layer are deduced from the depletion layer charge according to expressions (1) and (2). The charge versus bias

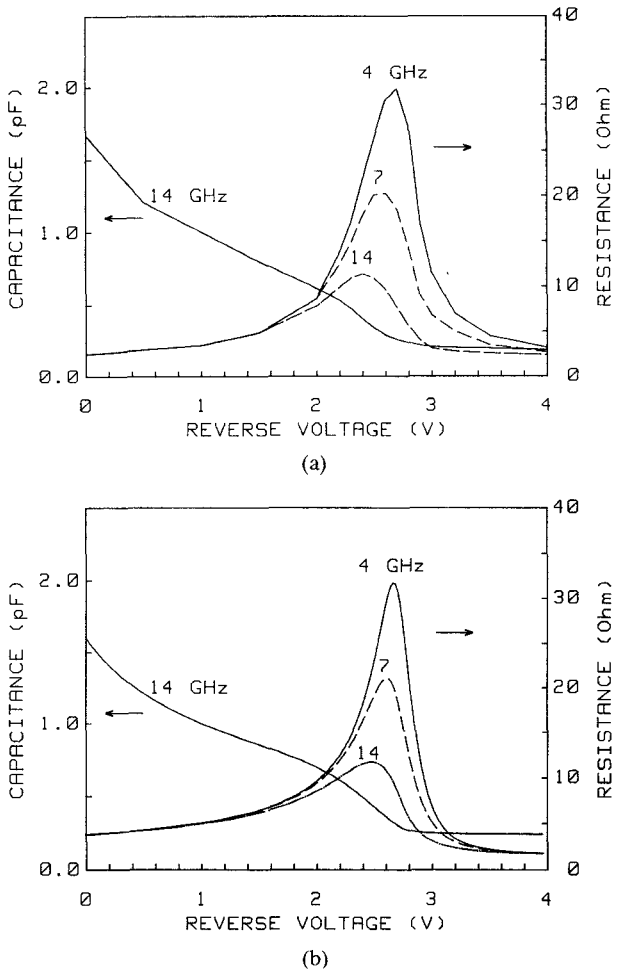

Fig. 10. (a) Measured and (b) simulated characteristics using large-signal model of a 4 μm × 240 μm varactor.

voltage variation is described by the following empirical expression:

$$Q = Q_0\left(1 - \frac{V_{\text{eff}}}{V_b}\right)^n \tag{16}$$

where Q_0, and n are adjustable parameters and V_{eff} is an effective control voltage that makes the charge saturate smoothly at pinch-off.

$$V_{\text{eff}} = 1/2\left(\sqrt{(V - V_t)^2 + \delta^2} - \sqrt{(V - V_b)^2 + \delta^2} + V_b + V_t\right) \tag{17}$$

with V_b and V_t, respectively, the built-in and pinch-off voltage, and δ the smoothing parameter. The extrinsic elements such as the access resistances, side-wall capacitance, and leakage conductance are assumed to be voltage independent. The input parameters of the model are the anode size (W, L) and the number of anode fingers. Fig. 10 shows an example of the measured and simulated characteristics of a varactor.

VI. Conclusions

A physical equivalent circuit model suitable for CAD which accounts for the frequency behavior of PSVD's up to pinch-off has been reported. The maximum series resis-

tance R_{max} near pinch-off decreases with anode width and frequency, and increases with anode length. Consequently, there is no optimum geometry for a PSVD with regard to the broad-band monolithic VCO constraints and a compromise has to be found between R_{max} and C_{min} on the one hand, and R_{max} and C_{max}/C_{min} on the other. Investigation of the influence of the doping profile has shown that R_{max} can be significantly decreased for a small-gate-length PSVD ($L \leqslant 5$ μm) by decreasing the doping gradient between the active layer and the semi-insulating substrate. Such a doping profile is unfortunately not suitable for FET's; therefore selective implantation is required to improve the PSVD and hence broad-band monolithic VCO's.

ACKNOWLEDGMENT

The authors wish to thank M. Renvoise for PSVD realization, J. Maluenda for ion implantation, J.-C. Meunier for technical assistance, and C. Kermarrec for helpful discussions.

REFERENCES

[1] G. E. Brehm, B. N. Scott, D. J. Seymour, W. R. Frensley, W. N. Duncan, and F. H. Doerbeck, "High capacitance ratio monolithic varactor diode," in *1981 Cornell Microwave Conf. Dig.*, pp. 53–63.

[2] B. N. Scott, G. E. Brehm, and F. H. Doerbeck, "*X*-band GaAs monolithic voltage controlled oscillators," in *ISSCC-82 Dig.*, 1982, pp. 138–139.

[3] B. N. Scott and G. E. Brehm, "Monolithic voltage controlled oscillator for *X*- and *Ku*-bands," *IEEE Trans. Microwave Theory Tech.*, vol. MTT-30, pp. 2172–2177, Dec. 1982.

[4] W. El-Kamali, J. P. Grimm, R. Meierer, and C. Tsironis, "New design approach for wide-band FET voltage controlled oscillators," *IEEE Trans. Microwave Theory Tech.*, vol. MTT-34, pp. 1059–1063, Oct. 1986.

✠

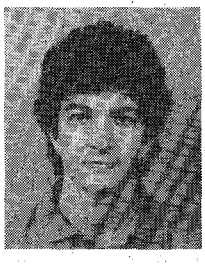

Pascal Philippe was born in France on August 28, 1959. He received the Docteur es Sciences degree in 1985 from the Université des Sciences et Techniques de Lille, France, for his work on optoelectronics in the Laboratoire Central de Recherche (Thomson CSF), Orsay, France.

He joined the Laboratoires d'Electronique et de Physique appliquée (a member of the Philips Research Organization) in 1985 and is now working on MMIC design and electron devices modeling.

✠

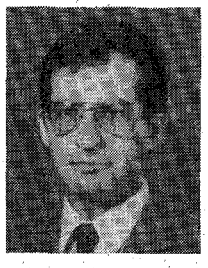

Walid El-Kamali was born in Tripoli, Lebanon, on January 7, 1959. He received the Maîtrise degree in electronics in 1981 from the University, of Toulouse, France, and the Diploma of Engineering in telecommunications in 1983 from the Ecole Nationale Supérieure de Télécommunications, in Paris. From 1980 to 1987 he was at the Laboratoires d'Electronique et de Physique appliquée (the Philips Research Laboratory in France), where he completed his doctoral thesis on the bandwidth limitations of broad-band monolithic voltage-controlled oscillators.

He is currently a postdoctoral fellow at the Ecole Polytechnique de Montreal, where he is involved in optoelectronics research.

✠

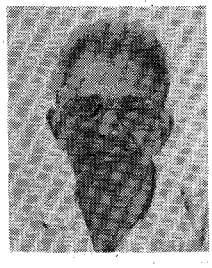

Vlad Pauker received the M.S. degree in electronic engineering from Bucharest Polytechnical Institute in 1952 and the Ph.D degree in 1957.

In 1957, he became a research scientist at the Institute of Nuclear Physics of the Rumanian Academy of Science. From 1956 to 1958, he was an Assistant Professor at the Bucharest Polytechnical Institute. In 1960, he founded the Solid State Device Application Laboratory of IPRS (Bucharest). In 1969, Dr. Pauker joined RTC in Paris, leading the development of solid-state microwave circuits. Since 1979, he has been working at LEP, Paris, where he now supervises the study of GaAs microwave monolithic integrated circuits.